Numerical Simulation of Annular Phased Arrays for Anatomically Based Models Using the FDTD Method

CHANG-QING WANG AND OM P. GANDHI, FELLOW, IEEE

Abstract—**Annular phased arrays (APA's) of aperture and diopole antennas used for hyperthermia are simulated in three dimensions by using the finite difference time-domain (FDTD) method. A 17 363 cell, 1.31 cm resolution, anatomically based model of the human torso surrounded by a bolus of deionized water is used for calculations of specific absorption rates (*SAR*'s). Test runs on the calculation of fields in the water-filled interaction space and with homogeneous circular- and elliptical-cylinder phantoms correlate well with the experimental data in the literature, lending support to the accuracy of the FDTD method for near-field exposure conditions. Results are given for APA's using different sizes of aperture and dipole antennas and for a subannular array to obtain higher SAR's in the liver. Because of its flexibility, the procedure of this paper may be useful for a variety of realistic radio frequency applicators for hyperthermia and other biomedical applications.**

I. Introduction

ONE OF THE greatest technical challenges faced by hyperthermia researchers has been the development of a means for selectively heating deep central tissues in the patient's body. A recent development capable of therapeutic heating in deep tumors is the annular phased array (APA) [1]–[3]. The APA's are constructed of TEM aperture sources or dipoles such that the dominant electric field vector of each aperture or the dipole is aligned with the axial center line of the annular opening, and this results in a cylindrical convergent radiation field pattern in that space. It is the objective of the APA to create reinforcement by constructive interference of the coupled energies from the individual sources at the location of the tumor.

Some results of distribution of power and temperature for APA's have been obtained experimentally using cylindrical, human-shaped homogeneous phantom models [1]–[3]. But the coupling of EM energy into the body is a highly complex process depending strongly on the inhomogeneities of the dielectric properties of the tissues and their location vis-à-vis the radiating elements of the array. Three-dimensional numerical methods which take into account the overall interaction of the body with electromagnetic fields are therefore required to model and accurately predict the distribution of the absorbed energy.

This paper presents some numerical results by using the three-dimensional finite difference time-domain (FDTD) method for simulating the interaction of fields from the APA's with circular- and elliptical-cylinder phantoms and a 17363 cell, 1.31 cm resolution, anatomically based model of the human torso.

In practice a dionized water bolus is typically used between the body and the radiating elements to improve field matching as well as to obtain superficial cooling. The modeled three-dimensional space is therefore considered filled with deionized water between the radiating elements and the lossy phantoms or the inhomogeneous model of the human torso. Test runs on the calculation of fields in the water-filled interaction space and with homogeneous circular- and elliptical-cylinder phantoms are compared with the experimental data to check the accuracy of the FDTD method. Results are given for the 14-tissue inhomogeneous model of the human torso for APA's with different sizes of aperture and dipole antennas and for a subannular array to obtain higher *SAR*'s in the liver.

II. Description of the Method

The finite difference time-domain (FDTD) method was first proposed by Yee [4] and later developed by Taflove [5]–[7], Holland [8], and Kunz *et al.* [9]. Recently it has been extended for calculations of the distribution of electromagnetic fields in a man model for incident plane waves [10], [11]. In the method, the time-dependent Maxwell's curl equations,

$$\nabla \times \boldsymbol{E} = -\mu \frac{\partial \boldsymbol{H}}{\partial t} \qquad \nabla \times \boldsymbol{H} = \sigma \boldsymbol{E} + \epsilon \frac{\partial \boldsymbol{E}}{\partial t} \tag{1}$$

are implemented for a lattice of cubic cells. The components of $\boldsymbol{E}$ and $\boldsymbol{H}$ are positioned about a unit cell of the lattice (see Fig. 1) and evaluated alternatively with half-time steps. The goal of the method is to model the propagation of an electromagnetic wave into a volume of space containing dielectric and/or conducting structures by time stepping, i.e., repeatedly implementing a finite difference analog of the curl equations at each cell of the corresponding space lattice. The incident wave is tracked as it propagates

Manuscript received December 23, 1987; revised July 27, 1988. This work was supported by the National Science Foundation under Grant EET–8714651.

The authors are with the Department of Electrical Engineering, University of Utah, Salt Lake City, Utah 84112.

IEEE Log Number 8824262.

0018-9480/89/0100-0118$01.00 ©1989 IEEE

to the dielectric structure and interacts with it via surface current excitation, spreading, penetration, and diffraction. Wave tracking is completed when sinusoidal steady-state behavior for $\boldsymbol{E}$ and $\boldsymbol{H}$ fields is observed for each lattice cell.

The Maxwell equations (1) can be rewritten as difference equations. We assume the media to be nonmagnetic, i.e., $\mu = \mu_0$, and the grid point of the space defined as (i, j, k) with coordinate $(i\delta, j\delta, k\delta)$, where δ is the cell size.

Upon substituting

$$\tilde{\boldsymbol{E}} = \frac{1}{2}\sqrt{\frac{\epsilon_0}{\mu_0}}\,\boldsymbol{E} \tag{2}$$

the equations in difference form for $\boldsymbol{E}_z$ and $\boldsymbol{H}_z$, for example, can be written [10] as

$$\begin{aligned}\tilde{E}_z^{n+1}(i,j,k+1/2) &= CA_z(i,j,k+1/2)\tilde{E}_z(i,j,k+1/2)\\ &\quad + CB_z(i,j,k+1/2)\begin{bmatrix} H_y^{n+1/2}(i+1/2,j,k+1/2) - H_y^{n+1/2}(i-1/2,j,k+1/2)\\ + H_x^{n+1/2}(i,j-1/2,k+1/2) - H_x^{n+1/2}(i,j+1/2,k+1/2)\end{bmatrix}\end{aligned} \tag{3}$$

$$\begin{aligned}H_z^{n+1/2}(i+1/2,j+1/2,k) &= H_z^{n-1/2}(i+1/2,j+1/2,k)\\ &\quad + \begin{bmatrix}\tilde{E}_x^n(i+1/2,j+1,k) - \tilde{E}_x^n(i+1/2,j,k)\\ + \tilde{E}_y^n(i,j+1/2,k) - \tilde{E}_y^n(i+1,j+1/2,k)\end{bmatrix}\end{aligned} \tag{4}$$

where

$$CA_z(i,j,k+1/2) = \left[1 - \frac{\sigma_z(i,j,k+1/2)\delta t}{2\epsilon_z(i,j,k+1/2)}\right]\cdot\left[1 + \frac{\sigma_z(i,j,k+1/2)\delta t}{2\epsilon_z(i,j,k+1/2)}\right]^{-1} \tag{5}$$

$$CB_z(i,j,k+1/2) = \frac{\epsilon_0}{4}\left[\epsilon_z(i,j,k+1/2) + \frac{\sigma_z(i,j,k+1/2)\delta t}{2}\right]^{-1} \tag{6}$$

where the superscript n denotes the time $n\delta t$ in terms of the incremental time or time step δt. The time step δt is determined by the cell size and must satisfy the stability condition [5]

$$v_{\max}\delta t < \left[\frac{1}{\delta x^2} + \frac{1}{\delta y^2} + \frac{1}{\delta z^2}\right]^{-1/2} \tag{7}$$

where $v_{\max}$ is the maximum wave phase velocity within the model. For the cubic cell model $\delta x = \delta y = \delta z = \delta$, the following relationship is usually taken:

$$\delta t = \frac{\delta}{2C_{\max}} \tag{8}$$

where $C_{\max}$ is the maximum velocity of electromagnetic waves in the interaction space. We have taken $C_{\max}$ corresponding to the velocity for electromagnetic waves in fat and bone.

The ϵ and σ may be different for E_x, E_y, and E_z in the inhomogeneous media because, as shown in Fig. 1, the components of $\boldsymbol{E}$ are not positioned at the same point for the same cell in Yee's algorithm. Thus we have $\epsilon_x, \epsilon_y, \epsilon_z, \sigma_x, \sigma_y$, and σ_z for each of the cells.

A basic problem with any finite difference solution of Maxwell's equations is a treatment of the field components at the lattice truncation. Because of the limited computer storage, the lattice must be restricted in size. Proper truncation of the lattice requires that any outgoing wave disappear at the lattice boundary without reflection during the continuous time stepping of the algorithm. An absorption boundary condition for each field component is therefore needed at the edge of the lattice. In this paper, the absorption boundary conditions in the second approximation derived by Mur [12] are used. The condition for E_z at $i = 1$, for example, can be written as

$$\begin{aligned}\tilde{E}_z^{n+1}(1,j,k+1/2) &= -\tilde{E}_z^{n-1}(2,j,k+1/2)\\ &\quad + \frac{C_l\delta t - \delta}{C_l\delta t + \delta}\left[\tilde{E}_z^{n+1}(2,j,k+1/2) + \tilde{E}_z^{n-1}(1,j,k+1/2)\right]\\ &\quad + 2\left(\frac{\delta}{C_l\delta t + \delta} - \frac{(C_l\delta t)^2}{\delta(C_l\delta_t + \delta)}\right)\left(\tilde{E}_z^n(1,j,k+1/2) + \tilde{E}_z^n(2,j,k+1/2)\right)\\ &\quad + \frac{(C_l\delta t)^2}{2\delta(C_l\delta t + \delta)}\begin{bmatrix}\tilde{E}_z^n(1,j+1,k+1/2) + \tilde{E}_z^n(1,j-1,k+1/2) + \tilde{E}_z^n(2,j+1,k+1/2)\\ + \tilde{E}_z^n(2,j-1,k+1/2) + \tilde{E}_z^n(1,j,k+3/2) + \tilde{E}_z^n(1,j,k-1/2)\\ + \tilde{E}_z^n(2,j,k+3/2) + \tilde{E}_z^n(2,j,k-1/2)\end{bmatrix}\end{aligned} \tag{9}$$

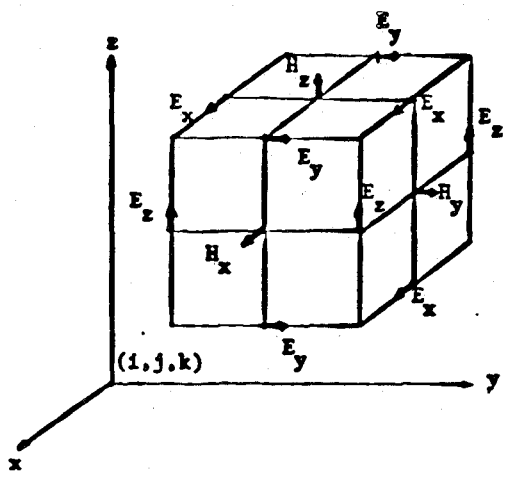

Fig. 1. A unit cell of the Yee lattice indicating the positions for the various field components.

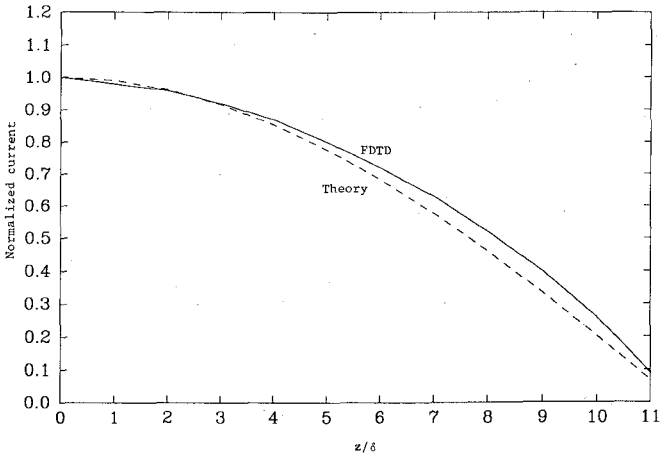

Fig. 3. FDTD-calculated current distribution for a "half-wave" dipole in free space versus theoretical variation. Length of dipole = 23δ (30.13 cm). Frequency = 500 MHz.

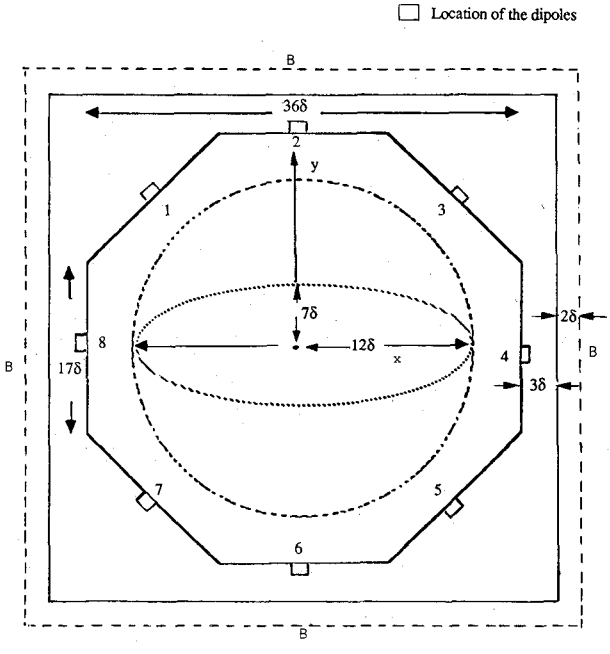

Fig. 2. Top view for the geometry of eight applicators including the positions of the circular and elliptical cylinder models in the interaction region for test runs. Height in the z direction = 55.02 cm (42δ) for test runs and 62.88 cm (48δ) for model of the torso. The exterior absorbing boundaries are shown by dashed lines B.

where C_l is the phase velocity observed at the lattice truncation, in our case corresponding to that for deionized water.

For simulating the APA, the various radiating elements, parallel-plate apertures or dipoles, are positioned at the proper places. The thickness of the plates or dipoles equals one cell size. For our calculations, the APA is represented by eight radiating elements, either parallel-plate apertures or dipoles. The top view for the example of the eight-aperture system is illustrated in Fig. 2, where the positions of the dipoles for the dipole-type APA's are also shown. The width of each aperture-type applicator is 17 cells (22.27 cm). The separation of the plates is variable and has been taken to be a couple of gaps, 34.23 cm (33δ) or 19.65 cm (15δ), respectively. Since the previously developed anatomically based model [11] was available with a cell size of 1.31 cm, the cell size δ for the various runs in this paper is taken to be 1.31 cm.

For TEM aperture APA's, a starting electric field with uniform amplitude and phase is assumed for the apertures of each of the parallel-plane radiating elements. The radiation fields from each of the apertures are traveling in two directions, i.e., to the central interaction space of the APA including the deionized water bolus, the absorbing body, and additional apertures, and away from this region where it is absorbed by the absorbing boundaries (indicated in Fig. 2). For the dipole-type elements, a uniform z-directed E field was assumed for the gap (taken to be 1δ) between the two arms assumed to be of equal length. This procedure for calculating near fields due to a dipole was validated by a test run of a half-wave dipole in air at 500 MHz. Starting with this prescribed uniform z-directed E field in the gap between the two equal arms, each of length 11δ (14.41 cm), the various components of $\boldsymbol{E}$ and $\boldsymbol{H}$ were calculated in the surrounding space. The conduction current at the various points of the dipole was obtained from the calculated tangential magnetic fields at the metallic sides of the dipole. The current thus obtained is compared with the expected sinusoidal variation of current in Fig. 3 and found to be in reasonable agreement. Several test runs were subsequently made for a variety of dipole lengths to check for the symmetry of the created fields in the water-filled interaction space. Upon finding a considerably broader distribution of fields for 29δ (37.99 cm) dipoles vis-à-vis 15δ (19.65 cm) dipoles (distance between half power points of 43.2 cm versus 27.5 cm), the latter were considered more desirable for the focused heating needed in hyperthermia. An eight-dipole APA, with each of the elements of length 15δ (19.65 cm), was therefore used for *SAR* calculations with the inhomogeneous model of the torso.

Similar to references [10] and [11], the inhomogeneous model of the human torso including part of the neck is

TABLE I
TISSUE TYPES USED IN CREATING THE TORSO MODEL, ALONG WITH THEIR MASS DENSITIES AND DIELECTRIC CONSTANTS AND CONDUCTIVITIES AT 100 MHz

Type of Tissue	Mass density 10^3 Kg/m^3	ε_r	σ(S/m)
Air	0.0012	1.0	0.0
Muscle	1 05	71.7	0.889
Fat/bone	1.20	7.5	0.067
Blood	1 00	74.0	1.1
Intestine	1.00	36.2	0.55
Cartilage	1.00	7.5	067
Liver	1.03	77.0	0.62
Kidney	1 02	90.0	1.01
Pancreas	1.03	90 0	1.01
Spleen	1.03	100.0	0.82
Lung (air-filled)	0.33	25.0	0 34
Heart	1.03	76.0	0.75
Nerve	1.05	82.0	0.53
Skin	1.00	24 5	0 55
Eye	1 00	85.0	1.90

taken from Eycleshymer and Schoemaker [13]. Their work contains cross-sectional diagrams of the human body which were obtained by making cross-sectional cuts at spacings of about 1 in in human cadavers. The process for creating the data base of the man model was the following. First a quarter-inch grid was taken for each single cross-sectional diagram and each cell on the grid was assigned a number corresponding to one of the 14 tissue types given in Table I [14]. Thus the data associated with a particular layer consisted of three numbers for each square cell: the x and y positions relative to the same anatomical reference point in this layer, usually the center of the spinal cord, and an integer indicating tissue which that cell contained. Since the cross-sectional diagrams available in [13] are for somewhat variable separations, typically 2.3–2.7 cm, a new set of equispaced layers were defined at quarter-inch intervals by interpolating the data onto these layers. Since a quarter-inch cell size is too small for the memory space of present-day computers, the proportion of each tissue type was calculated next for somewhat larger cells (half-inch) by combining the data for $2\times2\times2=8$ cells of the smaller dimension. Without changes in the anatomy, this process allows some variability in the height and weight of the body. We have taken a final cell size of 1.31 cm (rather than 1/2 in, or 1.27 cm) to obtain the whole-body weight of 69.6 kg for the model.

A three-dimensional region consisting of $46\times46\times42=88872$ unit cells was used in solving the problems with the cylinder models. For calculations with the partial-body man model a somewhat larger axial length was used and a volume consisting of $46\times46\times48=101568$ unit cells was taken. For all the cases the distance from one aperture to the opposite one was 36 cells, or 47.2 cm. (See Fig. 2.) The absorbing boundaries to contain the computation space are shown by dashed lines B in Fig. 2. Two absorbing lids parallel to the xy plane limit the computational space at the two ends of the z axis.

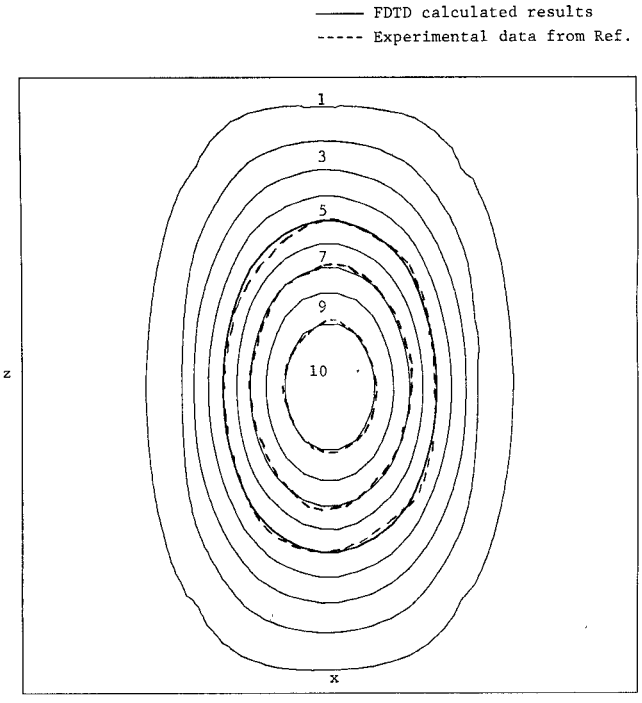

Fig. 4. Relative distribution of E^2 in the interaction region for the central vertical section when the interaction region is filled with deionized water. Dielectric constant = 78.0, conductivity = 0.0022 S/m. Frequency = 80 MHz. Aperture E field = 10 V/m for each of the radiating elements.

We have used a frequency of 100 MHz for the test runs with cylinder models and for the inhomogeneous torso model runs. The programs have been run on CRAY-2 and CRAY-XMP computers with run times typically on the order of 10 minutes.

III. RESULTS

In this section the results obtained by using the FDTD method to simulate the APA system in hyperthermia of the human body will be displayed. To understand the energy-focusing ability of the APA system, the distribution of electrical energy density is calculated in the first instance when the interaction space is filled with deionized water. For this case a dielectric constant of 78 and a conductivity of 0.0022 S/m are taken for deionized water at 80 and 100 MHz and 25°C. Fig. 4 shows the patterns of normalized power density in the interaction space filled with deionized water for the central vertical plane obtained by using the FDTD method and obtained by Turner experimentally [2] at 80 MHz. The agreement can be seen to be quite good. Additional calculations on the distributions of E^2 at 100 MHz in the horizontal (xy plane of Fig. 2) and vertical (yz) planes are shown in Figs. 5 and 6, respectively, for an incident field of 10 V/m for each of the apertures of opening 33δ, or 43.23 cm. The widths of half-power points for horizontal and vertical sections are

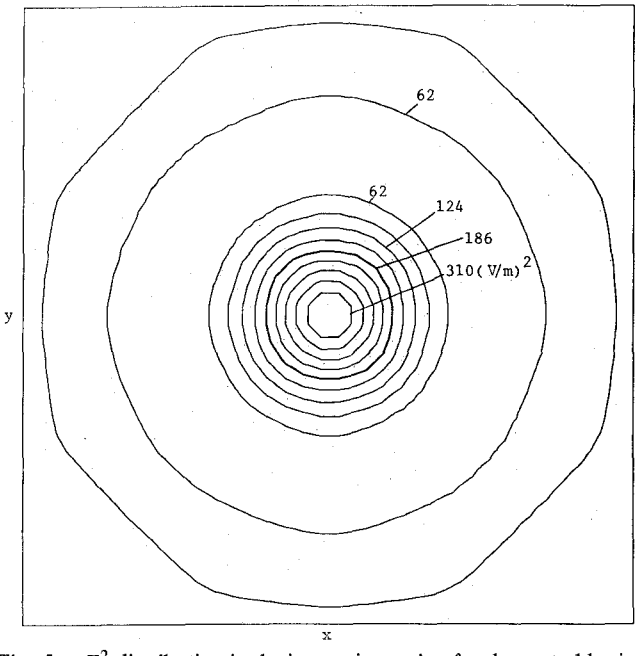

Fig. 5. E^2 distribution in the interaction region for the central horizontal plane when the whole interaction region is filled with deionized water. Frequency = 100 MHz; Aperture E field = 10 V/m for each of the radiating elements; step size between contours $\Delta = 31$ V^2/m^2.

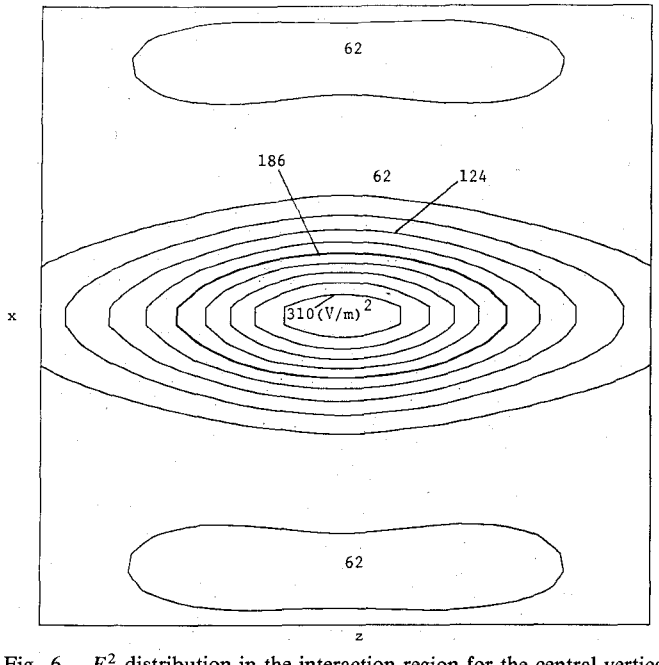

Fig. 6. E^2 distribution in the interaction region for the central vertical plane when the whole interaction region is filled with deionized water. Other parameters are the same as for Fig. 5. Step size between contours $\Delta = 31$ V^2/m^2.

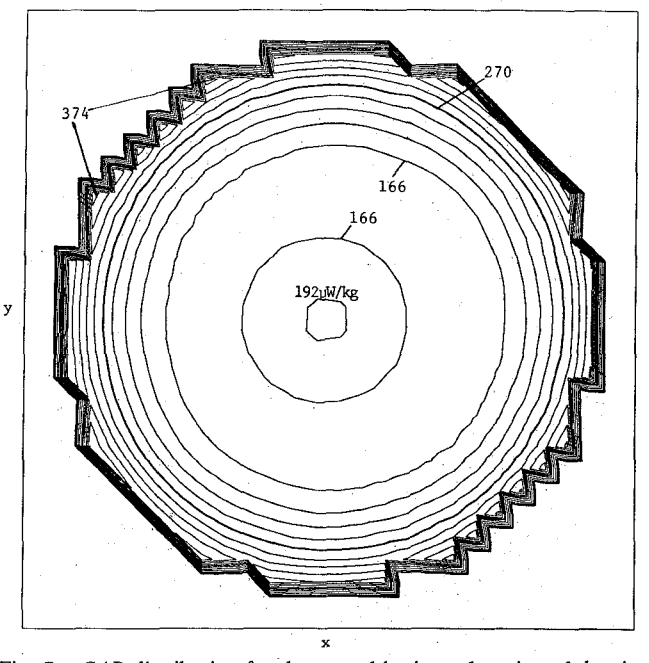

Fig. 7. *SAR* distribution for the central horizontal section of the circular cylinder model concentrically placed in the interaction space. Radius = 15.72 cm, dielectric constant = 47.8, conductivity = 0.593 S/m. Frequency = 100 MHz. Aperture E field = 1 V/m for each of the radiating elements. Step size between contours $\Delta = 26$ μW/kg.

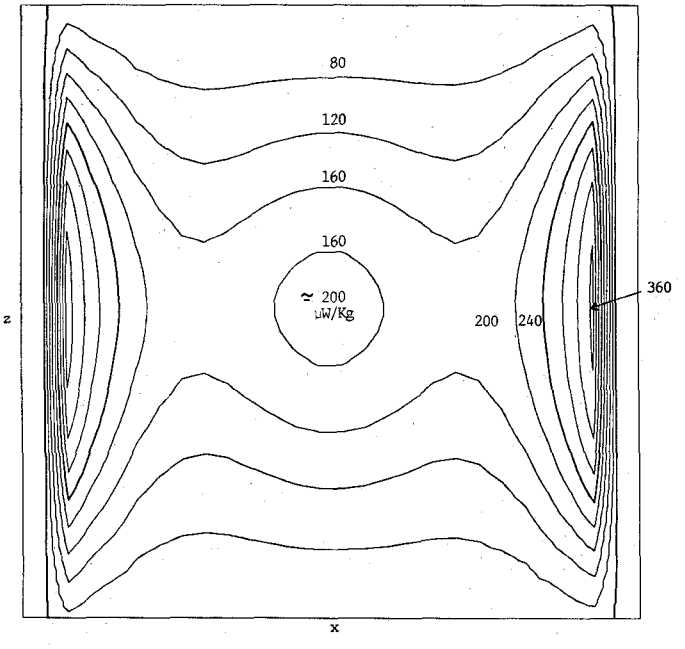

Fig. 8. *SAR* distribution for the central vertical section of the circular cylinder model. The various parameters are the same as for Fig. 7. Step size between contours $\Delta = 40$ μW/kg.

9.17 and 28.82 cm, respectively. The wavelength in water under these conditions is 33.97 cm.

The next test run used an absorbing circular cylinder having a dielectric constant of 47.8 and a conductivity of 0.593 S/m (2/3 of the value of dielectric constant and conductivity for muscle at 100 MHz) and a radius of 15.72 cm placed concentrically in the system (see Fig. 2). The calculated distribution of specific absorption rates (*SAR*'s) in the cylinder, given by $1/2\sigma E^2/\rho_m$, where ρ_m is the mass density, is shown in Figs. 7 and 8 for the horizontal and vertical planes, respectively. It can be seen that since the cylinder is absorptive, each of the waves decays along the radius of the cylinder, but also that there is a peak at the center due to the in-phase addition of the respective fields. An incident field of 1 V/m was taken for each of the apertures and a uniform mass density ρ_m of

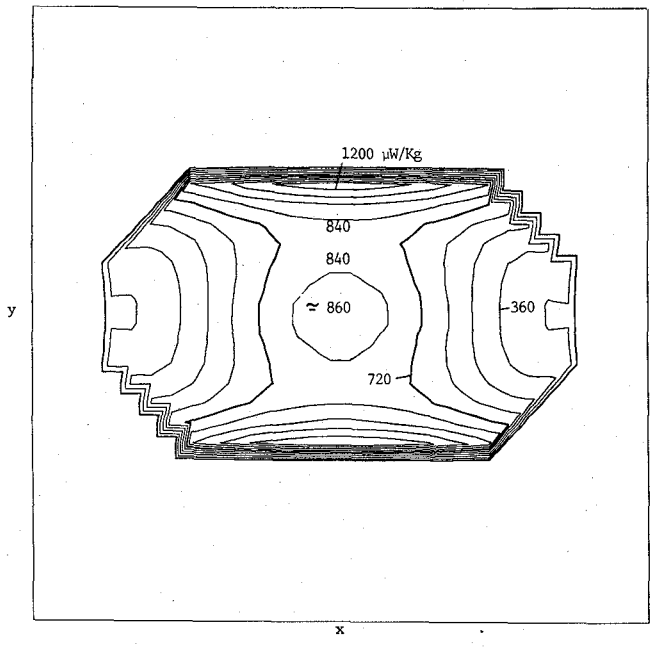

Fig. 9. *SAR* distribution for the central horizontal section of the elliptical cylinder model concentrically placed in the interaction space. Major axis = 31.44 cm, minor axis = 18.34 cm, dielectric constant = 47.8, conductivity = 0.593 S/m. Frequency = 100 MHz. Aperture E field = 1 V/m for each of the radiating elements. Step size between contours $\Delta = 120$ μW/kg.

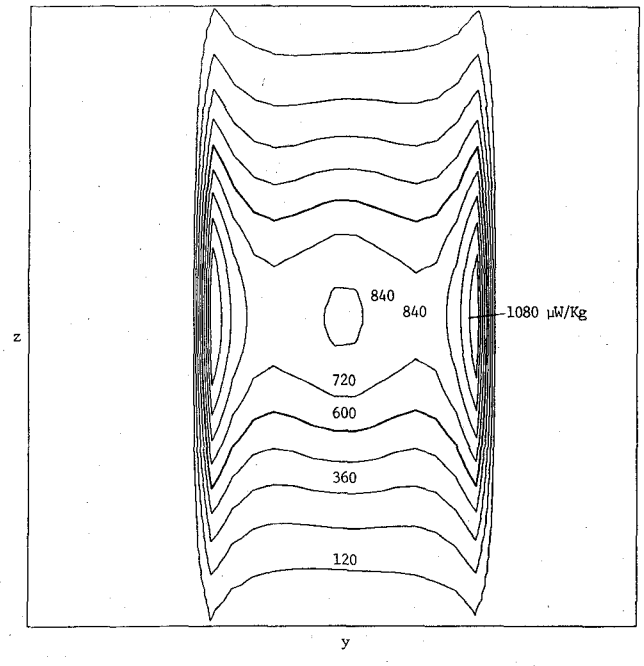

Fig. 10. *SAR* distribution for the *yz* section of the elliptical cylinder model. Other parameters are the same as for Fig. 9.

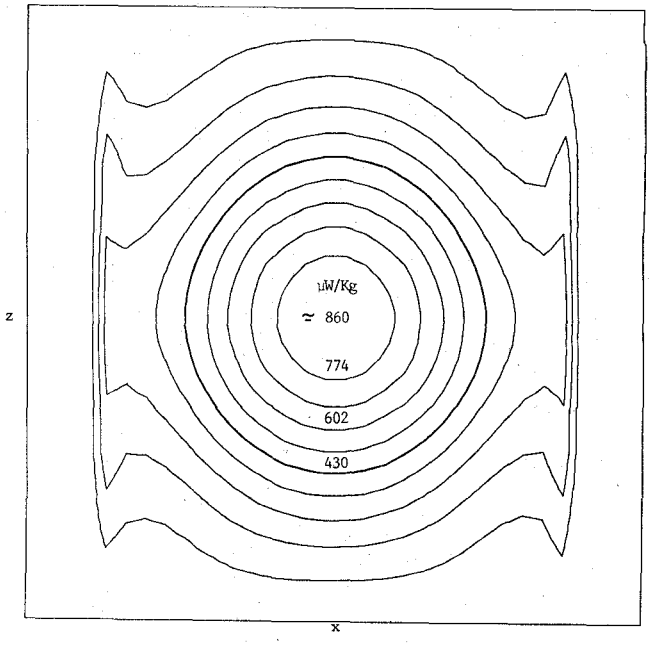

Fig. 11. *SAR* distribution for the *xy* section of the elliptical cylinder model. Other parameters are the same as for Fig. 9.

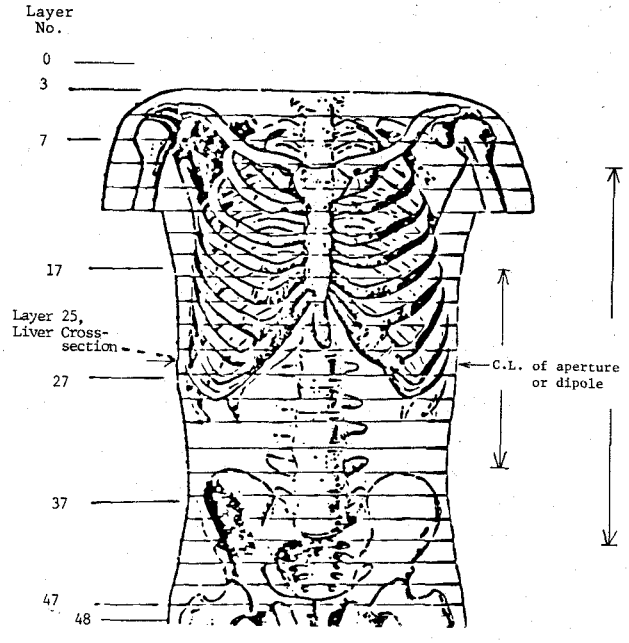

Fig. 12. Diagram of the human torso showing the levels at which data were calculated using the FDTD method. Also shown are the relative sizes of the apertures or dipoles.

1000 kg/m^3 was assumed for the results given in Figs. 7 and 8. Even though no plastic container for the cylinder was assumed for our calculations, the results in Figs. 7 and 8 are qualitatively very similar to those in [2].

Since the human torso is larger along one of the axes (side to side) than along the other axis, an elliptical cylinder model was also considered for a test run. The dimensions considered for the elliptical model along the x and y axes were 31.44 and 18.34 cm (24δ, 14δ), respectively. The calculated *SAR* distributions are shown in Figs. 9–11 for the *xy*, *yz*, and *xz* planes, respectively (see Fig. 2 for legend). Comparing the results with those for a circular cylinder (Figs. 7, 8) for identical irradiation parameters, one can see that the peak *SAR* obtained in the center is higher for the elliptical model than for the circular model —a property that would be useful for deep heating in hyperthermia.

The model of the torso used for *SAR* calculations for fields due to the APA's is shown in Fig. 12. Shown on the

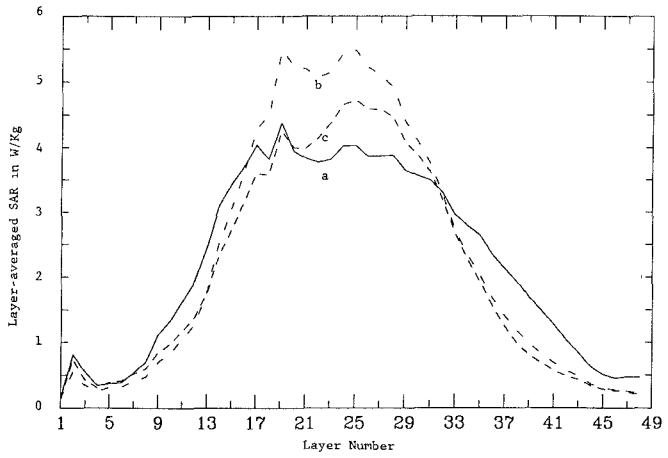

Fig. 13. Layer-averaged *SAR* distributions for the model of the torso: (a) eight parallel-plate applicators, each with a separation = 43.23 cm (33δ); (b) eight parallel-plate applicators, each with a separation = 19.65 cm (15δ); (c) elements 1–5 of Fig. 2 are energized, each with a separation = 19.65 cm (15δ). Frequency = 100 MHz. Input power = 100 W.

TABLE II
COUPLING EFFICIENCIES, AND MODEL- AND LIVER-AVERAGED SAR'S FOR THE VARIOUS APA'S. INPUT POWER = 100 W

APA	Coupling Efficiency percent	Model-averaged SAR W/kg	Average SAR for the liver W/kg
8 apertures separation = 43.23 cm (33δ)	87 5	2.25	3.04
8 apertures, separation = 19.65 cm (15δ)	90 7	2.48	7.01
Elements 1-5 (Fig. 2) are energized separation = 19.65 cm (15δ)	80.5	2.31	6.79

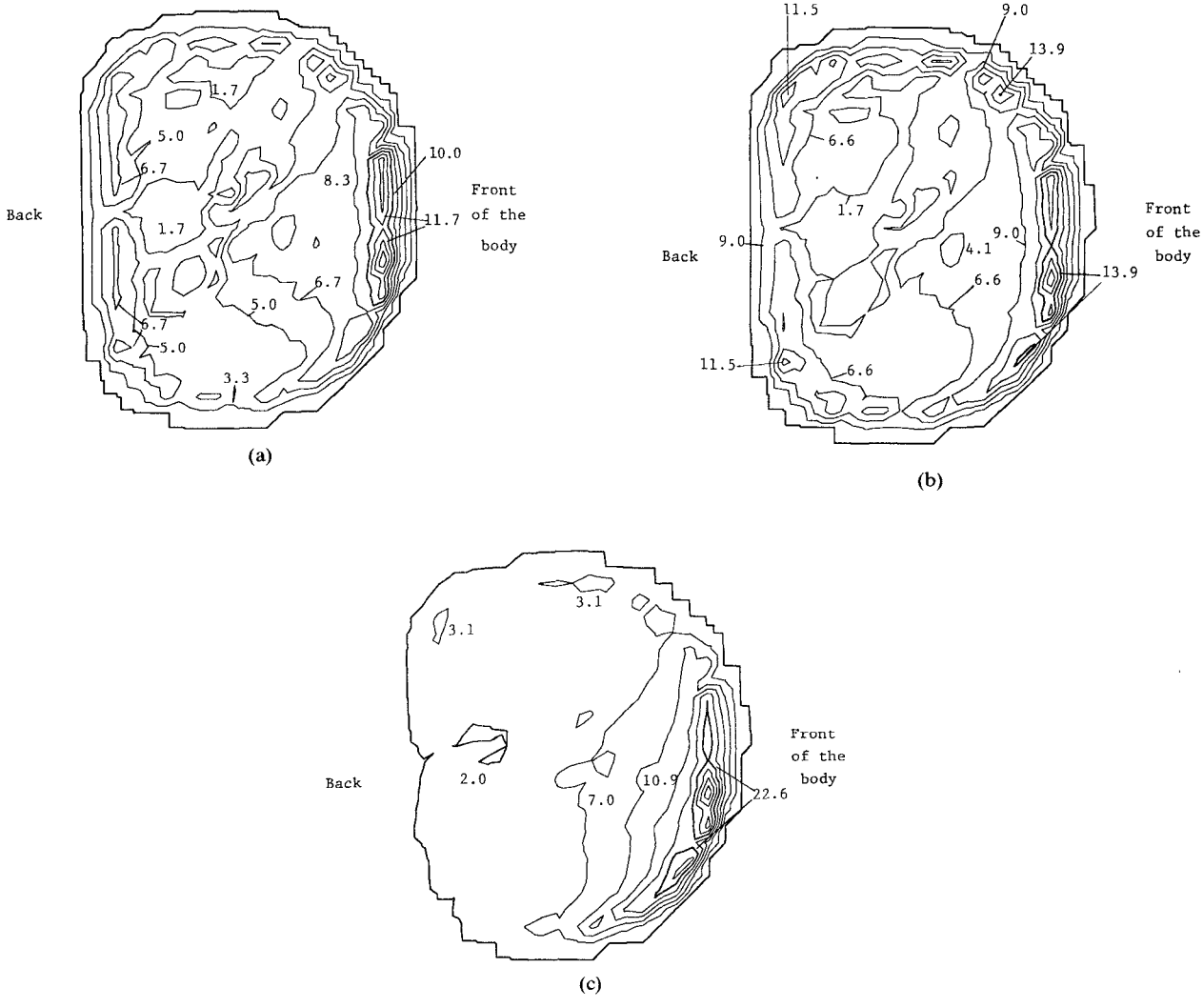

Fig. 14. *SAR* distributions for layer 25 corresponding to the central line of the applicators. (a) eight parallel-plate applicators, each with a separation = 43.23 cm (33δ). (b) eight parallel-plate applicators, each with a separation = 19.65 cm (15δ). (c) Elements 1–5 of Fig. 2 are energized, each with a separation = 19.65 cm (15δ). Frequency = 100 MHz. Input power = 100 W.

left are the layer numbers used for our model and for displaying the calculated *SAR*'s. Three cases have been considered for the parallel-plate applicators. In all cases the frequency is 100 MHz and the total incident power is 100 W.

In Fig. 13, the layer-averaged *SAR*'s are shown for the model of the torso for three cases: (a) eight radiating elements, each with a separation of 33δ, or 43.23 cm, (b) eight elements, each with a separation of 15δ, or 19.65 cm, and, (c) five elements (marked 1–5 in Fig. 2 on the side close to the liver to focus the energy preferentially into this organ. The mass densities for the various tissues given in Table I are used to calcualte the weights of the individual cells, which are then used to convert the volume densities $\sigma E^2/2$ of absorbed power to the *SAR*'s for the respective cells. The results are normalized for a total input power of 100 W. As expected, the energy absorption is more focused in the central layers for the narrower apertures of separation, 15δ, than for the wider aperture APA. The coupling efficiencies and the model-averaged and liver-averaged *SAR*'s of the various aperture-type APA's studied to date are given in Table II. As expected, proportionally higher *SAR*'s for the liver are obtained when the five elements closest to the liver are energized. The coupling efficiency for each of the cases is calculated from the total absorbed power for the model divided by the incident power. Fig. 14 gives the contours of the calculated *SAR*'s for layer #25, corresponding to the center line of the apertures for the various cases identified as (a), (b), and (c) above. Similar diagrams on the *SAR* distributions are, of course, available for each of the other layers as well.

Fig. 15 is a comparison of normalized layer-averaged *SAR*'s for the torso model for an eight-aperture APA (case (b) of Fig. 13) and an eight-dipole APA at a frequency of 100 MHz. Identical dipole length and aperture separations, each of 15δ, or 19.65 cm, have been used for the calculations. Consistent with experimental observations [15], fairly similar layer-averaged *SAR* distributions are calculated for aperture- and dipole-type APA's.

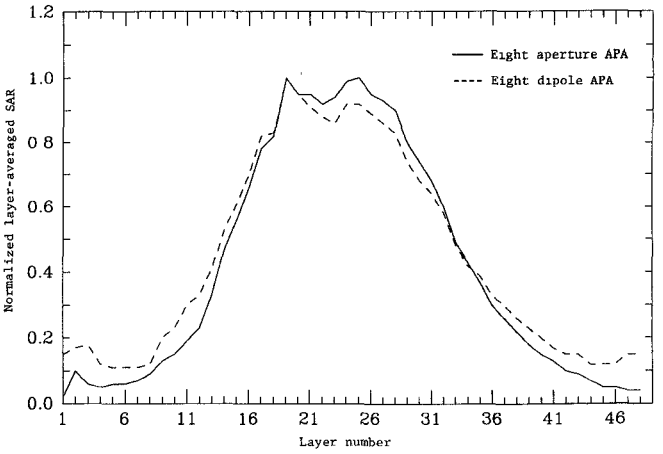

Fig. 15. Comparison of the normalized layer-averaged *SAR*'s for eight aperture and eight dipole APA's. Frequency = 100 MHz.

IV. Conclusion

The finite difference time-domain (FDTD) method has been used successfully in simulating *APA*'s of aperture and dipole antennas as individual elements. An anatomically based inhomogeneous model of the human torso surrounded by a bolus of deionized water is used for the *SAR* calculations. We have recently developed an anatomically based thermal block model of man [16] and have used it to date to calculate the temperature distributions for exposure to plane wave irradiation conditions. Since the cell sizes of this thermal model are compatible with those used here, the *SAR*'s obtained here could be used to calculate the temperature distributions for the various APA's. It will also be our goal in the future to use inhomogeneous models that are obtained from the CT scans of an individual patient so that the size and location of the tumor can be properly modeled. Using the procedure developed in this paper, one could then experiment with the size, location, amplitude, and phase of the various applicator elements for preferential heating of the tumor.

Acknowledgment

The authors acknowledge the many useful discussions with P. Turner of the BSD Medical Corporation.

References

[1] P. F. Turner, "Regional hyperthermia with an annular phased array," *IEEE Trans. Bio-Med. Eng.*, vol. BME-31, pp. 106–114, 1984.

[2] P. F. Turner, "Hyperthermia and inhomogeneous tissue effects using an annular phased array," *IEEE Trans. Microwave Theory Tech.*, vol. MTT-32, pp. 874–882, 1984.

[3] P. F. Turner, "Mini-annular phased array for limb hyperthermia," *IEEE Trans. Microwave Theory Tech.*, vol. MTT-34, pp. 508–513, 1986.

[4] K. S. Yee, "Numerical solution of initial boundary value problems involving Maxwell's equations in isotropic media," *IEEE Trans. Antennas Propagat.*, vol. AP-14, pp. 302–307, 1966.

[5] A. Taflove and M. E. Brodwin, "Computation of the electromagnetic fields and induced temperatures within a model of the microwave-irradiated human eye," *IEEE Trans. Microwave Theory Tech.*, vol. MTT-23, pp. 888–896, 1975.

[6] A. Taflove, "Application of the finite-difference time-domain method to sinusoidal steady-state electromagnetic-penetration problems," *IEEE Trans. Electromagn. Compat.*, vol. EMC-22, pp. 191–202, 1980.

[7] K. Umashankar and A. Taflove, "A novel method to analyze electromagnetic scattering of complex objects," *IEEE Trans. Electromagn. Compat.*, vol. EMC-24, pp. 397–405, 1982.

[8] R. Holland, "THREDE: A free-field EMP coupling and scattering code," *IEEE Trans. Nucl. Sci.*, vol. NS-24, pp. 2416–2421, 1977.

[9] K. S. Kunz and K-M Lee, "A three-dimensional finite-difference solution of the external response of an aircraft to a complex transient EM environment: Part 1—The method and its implementation," *IEEE Trans. Electromagn. Compat.*, vol. EMC-20, pp. 328–332, 1978.

[10] D. M. Sullivan, D. T. Borup, and O. P. Gandhi, "Use of the finite-difference time-domain method in calculating EM absorption in human tissues," *IEEE Trans. Bio-Med. Eng.*, vol. BME-34, pp. 148–157, 1987.

[11] D. M. Sullivan, O. P. Gandhi, and A. Taflove, "Use of the finite-difference time-domain method for calculating EM absorption in man models," *IEEE Trans. Bio-Med. Eng.*, vol. BME-35, pp. 179–186, 1988.

[12] G. Mur, "Absorbing boundary conditions for the finite-difference approximation of the time-domain electromagnetic field equations," *IEEE Trans. Electromag. Compat.*, vol. EMC-23, pp. 377–382, 1981.

[13] A. C. Eycleshymer and D. M. Schoemaker, *A Cross-Section Anatomy*. New York & London: D. Appleton, 1911.
[14] M. A. Stuchly and S. S. Stuchly, "Dielectric properties of biological substances—tabulated," *J. Microwave Power*, vol. 15, pp. 19–26, 1980.
[15] P. F. Turner, private communication.
[16] M. Hoque and O. P. Gandhi, "An inhomogeneous thermal block model of man for electromagnetic exposure conditions," submitted to *IEEE Trans. Bio-Med. Eng.*

✠

Chang-Qing Wang was born in Hebei Province, China. He graduated from the Department of Radio-Electronics of Peking University, Beijing, China, in 1960 and received the doctorate degree in physics and mathematical science from Kiev University, Kiev, Ukraine, U.S.S.R., in 1963.

He is an Associate Professor in the Department of Radio–Electronics, Peking University. His major research interests are in the theory of electromagnetic fields and microwave techniques. He has carried out research in parametric amplifiers, microwave integrated circuits, microstrip lines, dielectric waveguides, measurement methods of dielectric properties of biological materials at MW frequencies, and computer-aided analysis of bioelectric signals. In 1986–1987 he was a Research Associate in the Department of Electrical Engineering, University of Utah, Salt Lake City.

✠

Om P. Gandhi (S'57–M'58–SM'65–F'79) is a Professor of Electrical Engineering at the University of Utah, Salt Lake City. He is the author or coauthor of several book chapters, over 200 journal articles on microwave tubes, solid-state devices, and electromagnetic dosimetry and the textbook *Microwave Engineering and Applications* (New York: Pergamon).

Dr. Gandhi received the Distinguished Research Award from the University of Utah for 1979–1980 and a special award for "Outstanding Technical Achievement" from the IEEE, Utah Section, in 1975. He is Cochairman of the ANSI C95.4 Subcommittee on the RF Safety Standards (1988–) and a past Chairman of the IEEE Committee on Man and Radiation (COMAR). His name is listed in *Who's Who in the World*, *Who's Who in America*, *Who's Who in Engineering* and *Who's Who in Technology Today*.